


## Surface plasmonic Cherenkov radiation and symmetry breaking within a coherent nonlinear nanostructure

Saeid Asgarnazhad-Zorgabad 

Independent Researcher, West Ferdows Boulevard, Tehran 1483633987, Iran



(Received 31 May 2021; accepted 10 November 2021; published 22 November 2021)

Nonlinear conversions within the plasmonic structures are important for ultrafast nanophotonics; however, the impact of higher-order dispersion on nonlinear polaritonic efficiency remains unexplored. In this work, we uncover the role of higher-order dispersion and self-steepening on nonlinear surface-plasmon polaritons (NSPPs) within a coherent plasmonic interface that comprises an atomic medium doped on top of a low-loss negative-index metamaterial (NIMM) layer. This dispersion in the atomic medium–NIMM interface yields nonlinear plasmonic phase match and resonant launching of *Cherenkov* SPPs. We establish time-reversal and  $\mathcal{PT}$  symmetry breaking for propagated NSPPs that yield asymmetric plasmonic comb excitation and anomalous plasmonic phase singularities. Our work thereby suggests a fingerprint for nonlinear plasmonic field evolution through the appearance of a Cherenkov field and develops a framework for designing a *frequency selector* and nanoscopic pulse shaper, which opens prospects for nonlinear nanophotonic applications.

DOI: [10.1103/PhysRevA.104.L051503](https://doi.org/10.1103/PhysRevA.104.L051503)

**Introduction.** Nanoscopic nonlinear frequency conversions are of great interest due to their promising applications in on-chip frequency modulators [1], supercontinuum generation [2], and Stokes lasers [3]. Nonlinear field interactions within plasmonic nanostructures would yield frequency conversions [4] but the inclusion of higher-order dispersions and interface characteristics on nonlinear surface-plasmon polaritons (NSPPs) and frequency generations has not yet been explored. In this work, we uncover the role of third-order dispersion [5] and self-steepening [6] on polaritonic field evolution, report the appearance of plasmonic *Cherenkov* wave formation and anomalous phase singularities, and explore the application of this waveguide as a nanoscopic *frequency selector* [7].

The interplay between anomalous dispersion and self-focusing nonlinearity yields nonlinear wave formation that can emit Cherenkov radiation (CR) [8], which has been established within a nonlinear fiber with third-order dispersion (TOD) [9,10]. On the other hand, the interface between a low-loss metallic-like layer and a nonlinear medium generates NSPPs [11,12] that possess dissimilar propagation properties due to different field dispersions and nonlinear coefficients. Including second-order dispersion and self-focusing nonlinearity to SPP field evolution yields generation of different NSPP classes, from solitons to rogue waves, and from breathers to shock waves [4,11], which are symmetric in spatiotemporal and spatial-spectral domains. Among these works, the inclusion of higher-order dispersion and self-steepening to the dynamical evolution of NSPPs remains an open question. In this work, we uncover the role of these quantities in NSPPs and elucidate the appearance of plasmonic CR and symmetry breaking, which can only be obtained in a system with TOD and self-steepening.

**Model.** We consider a plasmonic waveguide comprising a nonlinear medium situated on top of a negative-index metamaterial (NIMM) layer. We coupled light to the waveguide using end-fire coupling technique [13] and employed a scattering scheme as the detection system. We assume coherent nonlinear interactions for which a cold atomic layer serves as a nonlinear medium, the NIMM layer acts as a low-loss medium, and fields excite the system as light sources. Our system can then be technically described as a *source-waveguide-detection* triplet. We assume a strong couple (c), switch (s), and weak probe (p) as source fields, all are linearly polarized, frequency stabilized, possess longer coherent time ( $\tau_L$ ) than the waveguide decay  $\tau_w$ , are spatially coherent  $l_L$  enough to cover the waveguide length  $l$ , and are prepared similar to Ref. [14] (see Fig. 1). Quantitatively, we describe the total electric field at the interface  $\mathbf{E}(\mathbf{r}, t)$  in terms of field components as  $\mathbf{E}(\mathbf{r}, t) = \sum_{l=c,s,p} \mathbf{E}_l \exp\{i\mathbf{K} \cdot \mathbf{r} - \omega_l t\}$ , which is tightly confined to the interface with  $\zeta_l(z)$  [11].

**Waveguide.** These laser fields excite a four-level  $N$ -type atomic medium (4NAs) that is appealing due to inducing Kerr nonlinearity and controllable dispersion to SPPs. Specifically, we consider  $\text{Pr}^{3+}$  ions with atomic density  $N_a$  that are doped as impurities within  $\text{Y}_2\text{SiO}_5$  crystals. Specifically, we choose  $|1\rangle = |^3H_4, \pm 5/2\rangle$ ,  $|2\rangle = |^3H_4, \pm 3/2\rangle$ ,  $|3\rangle = |^1D_2, \pm 3/2\rangle$ , and  $|4\rangle = |^1D_2, \pm 5/2\rangle$  as transition levels, whose natural decay rates are  $\Gamma_{mn}$  and dephasing rates are  $\gamma_{mn}^{\text{deph}}$ . Quantitatively, probe, couple, and signal fields with Rabi frequencies  $\Omega_l$  and frequency detunings  $\Delta_l$  drive  $|1\rangle \leftrightarrow |3\rangle$ ,  $|2\rangle \leftrightarrow |3\rangle$ , and  $|2\rangle \leftrightarrow |4\rangle$  respectively (see Fig. 1). The nonlinearity comes from this atomic medium. The atomic layer provides an electromagnetically induced transparency window satisfying vanished loss and giant nonlinearity; hereafter we term these conditions as *propagation requirements*, which support stable NSPPs. The control mechanism based on the atomic medium introduces coherence to NSPP

\*sasgarnazhad93@gmail.com

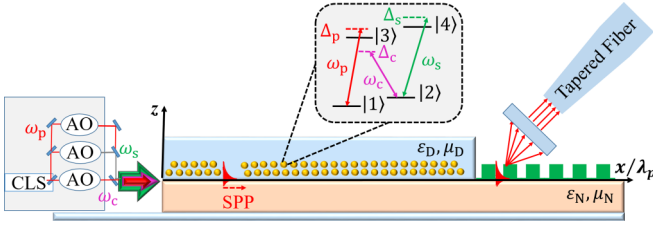


FIG. 1. Our proposed plasmonic scheme: This nonlinear waveguide comprises 4NAs (yellow dots) doped as a thin layer in a dielectric ( $\epsilon_D, \mu_D$ ) situated on top of a NIMM layer with ( $\epsilon_N, \mu_N$ ). Laser fields are obtained from a coherent laser source (CLS) and corresponding detunings are finely tuned using acousto-optic (AO) modulators.

propagation, and NSPPs excite using a low probe field power [11]. Exploiting coherent structures such as the atomic medium is one, nonunique way to obtain the NSPPs through the interaction interface. We note that any medium, such as multiple layers with nonlinear properties satisfying the propagation requirements, could serve as our upper layer.

Our aim in this work is to uncover the role of higher-order dispersion in NSPP propagation that can be excited in a waveguide that comprises a dielectric satisfying propagation requirements situated on top of a metallic-like layer. Among metallic layers, NIMM is an engineered structure with metallic-like properties and possessing ultralow Ohmic loss, and is suitable to support linear and nonlinear SPP waves, hence its inclusion is crucial to observe our predicted effects. We suggest a nanofishnet NIMM due to its efficiency for producing SPPs within the optical frequency range [15], and we establish Ohmic loss compensation using virtual gain, which is obtained by destructive interference of two contrapropagating fields for  $|1\rangle \leftrightarrow |3\rangle$  dipole transition wavelength [16]. We model the nanofishnet NIMM layer with electrical permeability  $\epsilon_N(\omega)$  and magnetic permeability  $\mu_N(\omega)$ , which is a macroscopic description of the metallic layer, following the Drude-Lorentz model [17,18]. The field within this surface becomes  $\zeta_l(z)\Omega_l$ , and we excite two contrapropagating SPP modes with controllable phase to achieve effectively zero imaginary part in the refractive index [19]. We note that our work using this ultralow NIMM layer is an extension to NSPP dynamics, which is observed only for such metallic interfaces. A nonlinear waveguide with a positive index instead of NIMM cannot support SPP waves and hence this layer is not suitable to predict our effects.

**Detection.** To detect output NSPPs, we suggest a programmable dielectric as a Bragg grating structure that scatters the output NSPP field for our preferable frequency range. The output field is evanescently coupled to a fiber and the output power collects using intensifiers and optical detection systems. Quantitatively, we model the output SPP waves as an evanescent field with  $\theta = \mathcal{K}(\omega) \cdot \mathbf{r} - (\omega + \omega_p)t$ , that propagates through the Bragg dielectric with a characteristic frequency that is in resonance with the NSPP frequency. For a scattered energy  $U_{\text{sca}}$  and reflected SPP field energy  $U_{\text{ref}}$ , the flux rate for SPP mode volume  $V = AL_B$  and for group velocity  $v_g$  is  $\Phi_j \sim U_j / (v_g(\lambda_j)V)$ ,  $j \in \{\text{sca}, \text{ref}\}$ , and the scattered ratio that propagates through the fiber is  $\eta_{\text{sca}}(\lambda_{\text{sca}}) \sim v_g(\lambda_{\text{sca}}) / v_g(\lambda_{\text{ref}})$ .

**Mathematical description of NSPPs.** SPPs excite with linear dispersion  $\mathcal{K}(\omega) = K(\omega) + k(\omega)$ . For frequencies around the spectral transparency window  $\omega_{\text{SPP}}$ , we employ  $\mathcal{K}(\omega) = \sum_{m=0}^{\infty} (\mathcal{K}_m/m!) (\omega - \omega_{\text{SPP}})^m$ ,  $\mathcal{K}_m = [\partial^m \mathcal{K}(\omega) / \partial \omega^m]$ .<sup>1</sup> Here  $\mathcal{K}_2$  and  $\mathcal{K}_3$  are group-velocity dispersion and TOD, respectively. NSPPs stably propagate through the interaction interface with self-focusing nonlinearity  $\mathcal{W}$  and with group velocity  $v_g(\omega) = [\partial \mathcal{K}(\omega) / \partial \omega]^{-1}$ . We introduce  $\epsilon = \min\{\Omega_p/\Omega_c, \Omega_p/\Omega_s\}$  as a perturbation parameter, we consider  $\bar{\alpha} = \epsilon^2 \text{Im}[\mathcal{K}(\omega)]$  as the loss related to this nonlinear waveguide, and  $\tau_0$  is the SPP's temporal pulse width. The NSPPs excite in the interface with nonlinear polarization  $\mathbf{P}_{\text{NL}}$ , with Rabi frequency  $U_0 = [\mathcal{K}_2/(\tau_0^2 \mathcal{W})]^{1/2}$ , and with characteristic dispersion length  $L_D = \tau_0^2/\mathcal{K}_2$ . We rescale the output NSPP field as  $u = \Omega_p/U_0$  and thereby the NSPPs stably propagate up to a few nonlinear lengths  $L_{\text{NL}} = (U_0^2 \mathcal{W})^{-1}$ . In this nonlinear waveguide, third-order dispersion would be relevant if the NSPPs propagate for characteristic length  $L_{\text{TOD}} = 6\tau_0^3/\mathcal{K}_3$ .

Next, we rescale the variables in spatiotemporal and spatial-spectral spaces in terms of NSPP parameters to achieve the dynamical evolution of the SPP field within this hybrid interface. To this aim, we choose the frequency grid as  $\iota := U_0$ , and rescale the spatial domain as  $s := x/L_{\text{NL}}$  and temporal domain as  $\sigma := \tau_0^{-1}(t - x/v_g)$ . We consider  $L_D \approx L_{\text{NL}}$  for dispersion-nonlinearity balance and stable NSPP formation, and define  $\Delta\omega = v_g \delta \mathcal{K}$  as the spectral deviation for which NSPP can stably propagate. The SPP noise related to this interface is  $\Delta u \ll u$ , the interface dissipation is  $u = [\Omega_p/U_0] \exp\{-\bar{\alpha}x\}$ , and finally we assume nonlinear dispersion of the system as  $\beta_{\text{NL}} \sim \mathcal{W}/(\omega_{\text{SPP}} u)$ . We achieve the nonlinear evolution related to this SPP field  $u := u(x, t)$  within this hybrid interface as

$$i \frac{\partial u}{\partial x} - \frac{\mathcal{K}_2}{2} \frac{\partial^2 u}{\partial \sigma^2} - i \frac{\mathcal{K}_3}{6} \frac{\partial^3 u}{\partial \sigma^3} - \beta_{\text{NL}} \frac{\partial(|u|^2 u)}{\partial \sigma} + |u|^2 u \approx \bar{\alpha} u. \quad (1)$$

Introducing TOD and  $\beta_{\text{NL}}$  affects the dynamical evolution of NSPP, which evidently differs from previous works [4,11,12] where only  $\mathcal{K}_2$  and  $\mathcal{W}$  were taken into account.

**Methods.** Our quantitative approach towards NSPP dynamics is based on Maxwell-Bloch equations that are represented in Ref. [21], and here we qualitatively describe this perturbative method for a nonlinear plasmonic interface. The temporal evolution of the atomic medium is obtained by the Liouville equation and we achieve the SPP field dynamics using the Maxwell equation, consequently we employ coupled Maxwell-Liouville equations to evaluate the propagation properties of the NSPPs. We then calculate the nonlinear dynamics by exploiting asymptotic expansion commensurate with slow-scale position  $x_l = \epsilon^l x$ ,  $l = \{0, 1, 2\}$  and slower scale time  $t_l = \epsilon^l t$ ,  $l = \{0, 1\}$  to Maxwell-Liouville equations, and we truncate the perturbative solution to fourth order to include the third-order and nonlinear dispersion effects.

<sup>1</sup> $k(\omega)$ , the propagation constant of SPP field can be obtained using boundary conditions [20] and we evaluate  $K(\omega)$  for this atomic system similarly to Ref. [11]. For more details related to this expansion see Refs. [11,12].

To simulate the spatiotemporal and spatial-spectral dynamics of NSPPs, we consider  $P_p$  as input power and consider  $u(x=0, t) = \sqrt{P_p} \psi(t) + \Delta u$  as initial condition of (1). Our simulation for this plasmonic waveguide with  $u(x=0, t)$  as initial condition is based on the split-step Fourier transform technique [22], for which we employ the impact of dispersion through temporal steps and nonlinearity through the spatial step to achieve  $u(x, t)$ , and we employ the dispersion through a frequency grid to evaluate the corresponds spatial-spectral evolution.

To test the feasibility of our scheme inreal-life experiment, we consider atomic density as  $N_a = 6 \times 10^{18} \text{ cm}^{-3}$ , radiative decays  $\Gamma_{31} = \Gamma_{42} \approx 9 \text{ KHZ}$ , and non radiative decay  $\Gamma_{31}^{(NR)} \approx 6 \text{ KHZ}$ . We also choose  $\Delta_c = 0.5 \text{ MHz}$ ,  $\Delta_p = 0 \text{ MHz}$ ,  $\Omega_c = 50 \text{ MHz}$ ,  $\Omega_s = 90 \text{ MHz}$ , and assume  $\Delta_s$  as a control parameter to tune the dispersion and nonlinearity. The SPP excitation frequency is  $\omega_{\text{SPP}} \approx 2\pi(4.95) \times 10^{14} \text{ s}^{-1}$ , and The plasmonic pulse width is  $\tau_0 = 0.6 \mu\text{s}^{-1}$ . We note that higher-order dispersions in our proposed interface  $\mathcal{K}_m$  would depend on Rabi frequencies, detunings, and relaxation rates of  $\text{Pr}^{3+}$ , and for these parameters we have  $\mathcal{K}_2 = (2.4 - 0.32i) \times 10^{-17} \text{ cm}^{-1}\text{s}^2$  and  $\mathcal{K}_3 = (7.69 + 0.28i) \times 10^{-22} \text{ cm}^{-1}\text{s}^3$ , and the nonlinearity coefficient is  $\mathcal{W} = (3.1 + 0.32i) \times 10^{-14} \text{ cm}^{-1}\text{s}^2$ . The NSPPs then propagate with a few nonlinear characteristic lengths in the presence of TOD and nonlinear dispersion.

*Plasmonic Cherenkov propagation.* Equation (1) uncovers a concept for the dynamical evolution of the SPP field, for which any input plasmonic field possesses deformation due to the existence of higher-order dispersions, and hence it is possible to generate new types of plasmonic waves. We proceed through NSPP evolution by considering plasmonic Peregrine waves  $\psi_P(x, t)$  and Akhmediev breathers  $\psi_{AB}(x, t)$ , and establish the appearance of new types of plasmonic field, which we termed plasmonic CR, through this hybrid interface. The SPP field undergoes nonlinear evolution with pulse shape  $\mathcal{U}$  and phase  $\vartheta = k_{\text{Ch}}(\omega)x - \omega\mathcal{T}$ ,  $\mathcal{T} := t - x/V_{\text{Ch}}(\omega)$  as

$$u(x, t) = \mathcal{U} \exp\{i\vartheta\}, \quad (2)$$

representing plasmonic CR within NSPP wings that propagates with group velocity  $V_{\text{Ch}}(\omega)$ , which is a single field for a Peregrine wave and periodic for Akhmediev breather excitation as shown in Figs. 2(a) and 2(c). We write the corresponding wave number of this NSPP field as

$$k_{\text{Ch}}(\omega) := k_{\text{Ch}}^{\text{L}}(\omega) + k_{\text{Ch}}^{\text{NL}}(\omega) + \mathcal{K}(\omega). \quad (3)$$

We evaluate  $k_{\text{Ch}}^{\text{L}}(\omega)$  by plugging (2) into (1), and rewrite the nonlinear part as  $k_{\text{Ch}}^{\text{NL}}(\omega) = 1/L_{\text{NL}} + k_l^{\text{NL}}(x, t)$  for  $k_l^{\text{NL}}(x, t) := [\partial\phi_l(x, t)/\partial x]$  and with  $\phi_l(x, t)$  the phase evolution of the NSPP fields. We achieve this phase and consequently  $k_{\text{Ch}}^{\text{NL}}(\omega)$  by assuming a nonlinear plasmonic field as  $\mathbf{E}_{l,\text{SPP}}(\mathbf{r}, t) = \xi_l(x, t)\mathbf{E}_{\text{SPP}}^{\text{L}}(\mathbf{r}, t)$  whose nonlinear form factor  $\xi_l(x, t) = |\xi_l(x, t)| \exp\{i\phi_l(x, t)\}$  in the low-dispersion limit  $\mathcal{K}_{l>1} \mapsto 0$  is

$$\nabla \xi_l(x, t) = -i \frac{\omega_{\text{SPP}}^2 \mu_0}{2k_p n_{\text{eff}}} \frac{\int dz P_{l,\text{NL}} E_{\text{SPP}}^{\text{L}}(\mathbf{r}, t)}{\int dz |\mathbf{E}_{l,\text{SPP}}(\mathbf{r}, t)|^2}. \quad (4)$$

Consequently, Cherenkov SPPs appear due to higher-order dispersion, and nonlinear plasmonic phase match  $k_{\text{Ch}}^{\text{NL}}(\omega)$  and

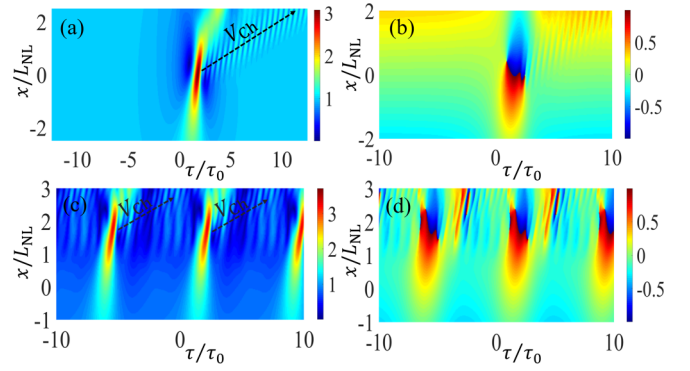


FIG. 2. Panel (a) is the dynamics of SPP Peregrine waves in the presence of TOD, and (b) represents the phase evolution of the plasmonic Peregrine wave. Panels (c) and (d) are the amplitude and phase dynamics of the SPP Akhmediev breathers. We termed the SPP waves that appeared as CR.

its single or periodic field modulations depend on the spatiotemporal evolution of NSPPs, as is shown in Figs. 2(b) and 2(d). CR would then stably propagate through the interface with a group velocity  $V_{\text{Ch}}(\omega) := [\partial k_{\text{Ch}}(\omega)/\partial \omega]^{-1}$ . Quantitatively, this radiation or equivalently considering higher-order dispersion introduces time-dependent terms to (1) that affect the temporal symmetries, and hence breaking time-symmetry can be expected through plasmonic CR. Our simulations also establish that the plasmonic Cherenkov field introduces asymmetries in the temporal domain and its excitation breaks the temporal symmetry, for both plasmonic field amplitude [see Figs. 2(a) and 2(c)] and phase [see Figs. 2(b) and 2(d)], which was preserved for unperturbed Peregrine wave and breathers. Hereafter we termed this breaking as time-reversal symmetry breaking. Cherenkov SPPs appear due to plasmonic pulse compression and propagate as a singular point to NSPP, consequently the stable propagation of this Cherenkov plasmonic field should affect the NSPP dynamics. The spectral dynamics for a plasmonic Peregrine field represents CR  $\omega_{\text{Ch}}$  with narrow linewidth  $\delta\omega_{\text{Ch}}$  that propagates as a wing of the unperturbed Peregrine wave and Akhmediev breather, as shown in Figs. 3(a) and 3(c) respectively. Appearance of Cherenkov SPP is conceptually similar for both Peregrine and Akhmediev breather excitation as both pulsations experience the same dispersion and nonlinearity; however, interestingly, CR for the Akhmediev breather generates additional sidebands  $\omega \pm \delta\omega_{\text{Ch}}$  that arise due to time-periodic pulsation [i.e., Fig. 2(c)] and modulation instability, as clearly shown within  $2.1\omega_0 < \omega < 2.7\omega_0$  spectral windows in Fig. 3(c). Generally, CR yields plasmonic pulse deformation, and symmetry breaking in the spatial-spectral domain, and the Cherenkov excitation hence would destroy the plasmonic phase singularities and induce plasmonic amplitude asymmetries through both spatiotemporal and spatial-spectral symmetry breaking, as shown in Figs. 2 and 3. Spatiotemporal symmetry breaking is an extension of temporal symmetry breaking and is expected, as temporal and spatial evolution of NSPPs are coupled through inclusion of higher-order dispersion terms in (1). Consequently, any symmetry breaking in the temporal domain would also introduce symmetry breaking in the spatial domain. We refer to this symmetry breaking as  $\mathcal{PT}$  breaking.

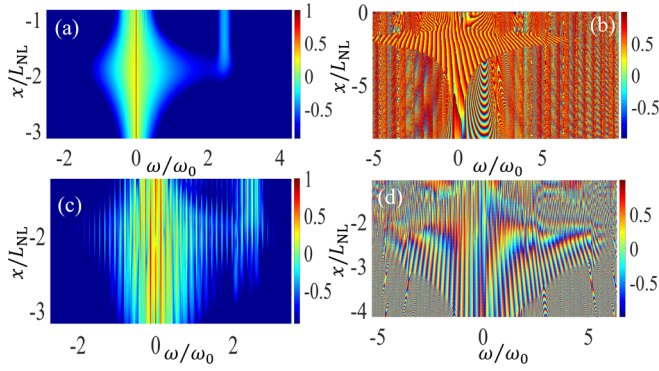


FIG. 3. Panels (a) and (b) represent the spectral amplitude and phase of the NSPPs, respectively, for SPP Peregrine wave excitation and panels (c) and (d) denote the spectral-sideband excitation and breather formation in the presence of higher-order dispersion. CR appears as wings of a stretched spectral plasmonic pulse, and propagates as frequency combs for breather wave excitation.

To evaluate  $\omega_{\text{Ch}}$ , we rewrite (3) as  $k_{\text{Ch}}^L + \mathcal{K}(\omega) = \delta k_{\text{NL}}$ , which is a phase-matching condition for characterizing Cherenkov excitation frequency. We then use  $k_{\text{Ch}}^L = (\mathcal{K}_3/6)\omega^3 + (\mathcal{K}_2/2)\omega^2 - (v_g + \beta_{\text{NL}})\omega$  and perform Taylor expansion to SPP field  $\mathcal{K}(\omega) = \mathcal{K}_0 + \mathcal{K}_1\omega + (\mathcal{K}_2/2)\omega^2 + O(\omega^3)$ . Plugging into the phase-matching condition and solving in terms of  $\omega$ , we achieve the CR frequency. Here, for SPP exciting with group velocity  $v_g = 2.34 \times 10^{-4}c$ ,<sup>2</sup> and with  $\omega_0 = 5$  MHz, we achieve  $\omega_{\text{Ch}} \approx 9.9$  MHz for both Peregrine and Akhmediev breathers, and CR propagates with  $V_{\text{Ch}} \approx v_g$ . This pulse introduces a propagating defect mode to the spectral dynamics, and hence its appearance breaks the spectral phase singularities that appeared due to unperturbed plasmonic Peregrine and Akhmediev breather fields. The spectral phase corresponding to NSPP propagation represents a distortion and asymmetric profile within  $2.1\omega_0 < \omega < 2.7\omega_0$  compared to its negative frequency deviation, which represent the Cherenkov field creation and spectral phase singularity distortions. Singularity breaking and asymmetric phases are shown in Figs. 3(b) and 3(d).

*Harmonic sideband and frequency selection.* Our excited SPP fields interact with focusing nonlinearity and second- and third-order dispersions, and, consequently, the propagated plasmonic waves generate sidebands as  $\omega = \pm n\Omega$  that yield frequency comb excitation for both Peregrine and Akhmediev breather waves, as depicted in Figs. 4(a) and 4(b), respectively. The spectrum corresponds to the plasmonic Peregrine wave and Akhmediev breather excitation, justifying the existence of CR; however its corresponding frequency can be tuned via the third-order dispersion term. In our numeric simulations, the Cherenkov frequency for  $\mathcal{K}_3 = (1.92 + 0.07i) \times 10^{-22} \text{ cm}^{-1}\text{s}^2$  is  $\omega \approx 2.48\omega_0$  and for  $\mathcal{K}_3 = (2.31 + 0.08i) \times 10^{-22} \text{ cm}^{-1}\text{s}^2$  is  $\omega \approx 1.38\omega_0$ .

To expand our method, we also include the noise as a plasmon mode with perturbation frequency  $\nu_{\text{mod}}$

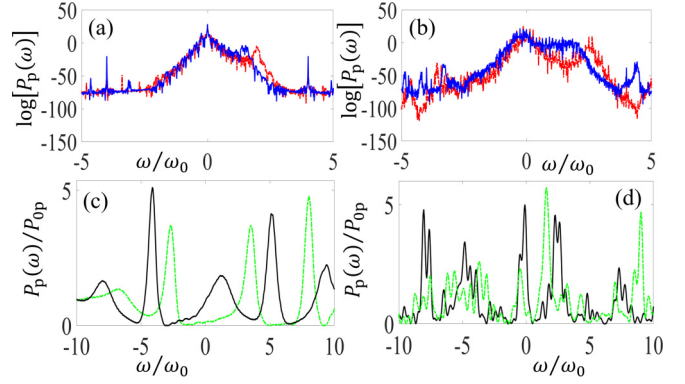


FIG. 4. Panels (a) and (b) represent the logarithmic power ( $\log[P(\omega)] := \log_{10}[P(\omega)]$ ) of NSPPs. Panels (c) and (d) are output NSPP pulses that we obtained using the transmission function approach. In both blue solid [panel (a)] and black solid [panel (c)] lines we have used  $\mathcal{K}_3 = (2.31 + 0.08i) \times 10^{-22} \text{ cm}^{-1}\text{s}^2$ , and for dotted-dashed red [panel (a)] and dotted-dashed green [panel (c)] curves we set  $\mathcal{K}_3 = (1.92 + 0.07i) \times 10^{-22} \text{ cm}^{-1}\text{s}^2$ . For panel (c)  $\nu_{\text{mod}} = 0.5\omega_{\text{SPP}}$  and for panel (d)  $\nu_{\text{mod}} = 0.415\omega_{\text{SPP}}$ .

and amplitude  $\Delta u = 0.08u_0$  as  $\Omega_p(\varepsilon, t) = \sqrt{P_p}(1 + \Delta u \cos\{2\pi\nu_{\text{mod}}t\})\psi_l(x, t)$ , and employ expansion to  $\omega(\mathcal{K})$ . We then use the transmission function approach [23] commensurate with third-order and nonlinear dispersion terms to evaluate  $\Omega_p(x, t) := \int d\omega T(x, \omega)\Omega_p(x = \varepsilon, t) \exp\{i\omega(\mathcal{K})t\}$ . Our simulations indicate that the higher-order dispersion terms affect the output NSPP pulse and the system selects specific frequencies by tuning the third-order parameter term, as clearly represented in Figs. 4(c) and 4(d), for both Peregrine and Akhmediev breather excitations. The output NSPP consequently is a pulse-shaped signal and preferred frequencies propagate through tuning the third-order dispersion term, and hence our device can act as a nanoscopic *frequency selector* or pulse shaper.

*Conclusion.* To sum up, we developed a concept that exploits spatiotemporal and spectral-spatial control of NSPPs to excite and propagate plasmonic CR. These waves appear in our designed nonlinear waveguide that comprises  $\text{Pr}^{3+}:\text{Y}_2\text{SiO}_5$  crystal, situated as a thin layer on top of an ultralow loss NIMM layer. We uncover that the third-order dispersion term introduces a nonlinear mismatch to the SPP field and breaks the spectral and temporal symmetries of the system, which is an origin for launching Cherenkov SPPs. Also, we justify that Cherenkov SPP is a single pulsation or periodic field that excites within temporal wings of the NSPPs, which generates additional harmonic sidebands as frequency combs for plasmonic Akhmediev breather propagation. Our numerical simulations indicate that the excitation frequency of CR is controllable, and can be coherently tuned via manipulation of detuning and intensity of driving laser fields. Finally, we established that the presence of TOD in a nanoscopic nonlinear system modifies the output spectral SPP field and we explored our designed waveguide's application to a frequency selector and pulse shaper, a concept that, for the plasmonic system, would open prospects for selective ultrafast nanophotonics and frequency modulators.

<sup>2</sup>Here  $c$  is the speed of light in vacuum.

- [1] A. L. Gaeta, M. Lipson, and T. J. Kippenberg, Photonic-chip-based frequency combs, *Nat. Photonics* **13**, 158 (2019).
- [2] D. Martyshkin, V. Fedorov, T. Kesterson, S. Vasilyev, H. Guo, J. Liu, W. Weng, K. Vodopyanov, T. J. Kippenberg, and S. Mirov, Visible-near-middle infrared spanning supercontinuum generation in a silicon nitride ( $\text{Si}_3\text{N}_4$ ) waveguide, *Opt. Mater. Express* **9**, 2553 (2019).
- [3] B.-B. Li, Y.-F. Xiao, M.-Y. Yan, W. R. Clements, and Q. Gong, Low-threshold Raman laser from an on-chip, high- $Q$ , polymer-coated microcavity, *Opt. Lett.* **38**, 1802 (2013).
- [4] S. Asgarneshad-Zorgabad and B. C. Sanders, Nonlinear frequency conversions via weak surface polaritonic wave breaking in a hybrid plasmonic waveguide, *Opt. Lett.* **45**, 5432 (2020).
- [5] F. Baronio, S. Chen, and S. Trillo, Resonant radiation from Peregrine solitons, *Opt. Lett.* **45**, 427 (2020).
- [6] F. DeMartini, C. H. Townes, T. K. Gustafson, and P. L. Kelley, Self-steepening of light pulses, *Phys. Rev.* **164**, 312 (1967).
- [7] M. Kourogi, K. Nakagawa, and M. Ohtsu, Wide-span optical frequency comb generator for accurate optical frequency difference measurement, *IEEE J. Quantum Electron.* **29**, 2693 (1993).
- [8] N. Akhmediev and M. Karlsson, Cherenkov radiation emitted by solitons in optical fibers, *Phys. Rev. A* **51**, 2602 (1995).
- [9] M. Erkintalo, Y. Q. Xu, S. G. Murdoch, J. M. Dudley, and G. Genty, Cascaded Phase Matching and Nonlinear Symmetry Breaking in Fiber Frequency Combs, *Phys. Rev. Lett.* **109**, 223904 (2012).
- [10] M. Conforti and S. Trillo, Radiative effects driven by shock waves in cavity-less four-wave mixing combs, *Opt. Lett.* **39**, 5760 (2014).
- [11] S. Asgarneshad-Zorgabad, R. Sadighi-Bonabi, and B. C. Sanders, Excitation and propagation of surface polaritonic rogue waves and breathers, *Phys. Rev. A* **98**, 013825 (2018).
- [12] S. Asgarneshad-Zorgabad, P. Berini, and B. C. Sanders, Polaritonic frequency-comb generation and breather propagation in a negative-index metamaterial with a cold four-level atomic medium, *Phys. Rev. A* **99**, 051802(R) (2019).
- [13] P. Berini, Long-range surface plasmon polaritons, *Adv. Opt. Photon.* **1**, 484 (2009).
- [14] H.-H. Wang, A.-J. Li, D.-M. Du, Y.-F. Fan, L. Wang, Z.-H. Kang, Y. Jiang, J.-H. Wu, and J.-Y. Gao, All-optical routing by light storage in a  $\text{Pr}^{3+}:\text{Y}_2\text{SiO}_5$  crystal, *Appl. Phys. Lett.* **93**, 221112 (2008).
- [15] V. M. Shalaev, Optical negative-index metamaterials, *Nat. Photonics* **1**, 41 (2007).
- [16] A. Ghoshroy, Şahin K. Özdemir, and D. O. Güney, Loss compensation in metamaterials and plasmonics with virtual gain [Invited], *Opt. Mater. Express* **10**, 1862 (2020).
- [17] S. Xiao, U. K. Chettiar, A. V. Kildishev, V. P. Drachev, and V. M. Shalaev, Yellow-light negative-index metamaterials, *Opt. Lett.* **34**, 3478 (2009).
- [18] A. Kamli, S. A. Moiseev, and B. C. Sanders, Coherent Control of Low Loss Surface Polaritons, *Phys. Rev. Lett.* **101**, 263601 (2008).
- [19] M. Sadatgol, S. K. Özdemir, L. Yang, and D. O. Güney, Plasmon Injection to Compensate and Control Losses in Negative Index Metamaterials, *Phys. Rev. Lett.* **115**, 035502 (2015).
- [20] C. Tan and G. Huang, Surface polaritons in a negative-index metamaterial with active Raman gain, *Phys. Rev. A* **91**, 023803 (2015).
- [21] C. M. Bowden and J. P. Dowling, Near-dipole-dipole effects in dense media: Generalized Maxwell-Bloch equations, *Phys. Rev. A* **47**, 1247 (1993).
- [22] X. Antoine, W. Bao, and C. Besse, Computational methods for the dynamics of the nonlinear Schrödinger/Gross-Pitaevskii equations, *Comput. Phys. Commun.* **184**, 2621 (2013).
- [23] J. Geng, G. T. Campbell, J. Bernu, D. B. Higginbottom, B. M. Sparkes, S. M. Assad, W. P. Zhang, N. P. Robins, P. K. Lam, and B. C. Buchler, Electromagnetically induced transparency and four-wave mixing in a cold atomic ensemble with large optical depth, *New J. Phys.* **16**, 113053 (2014).